ENVIRONMENTAL RESEARCH
LETTERS

LETTER • OPEN ACCESS

Detection of NO_2 pollution plumes from individual ships with the TROPOMI/S5P satellite sensor

Environmental Research Letters

LETTER

Detection of NO_2 pollution plumes from individual ships with the TROPOMI/S5P satellite sensor

Aristeidis K Georgoulias[1,2], K Folkert Boersma[1,3], Jasper van Vliet[4], Xiumei Zhang[5], Ronald van der A[1,5], Prodromos Zanis[2] and Jos de Laat[1]

[1] Royal Netherlands Meteorological Institute (KNMI), De Bilt, The Netherlands
[2] Department of Meteorology & Climatology, Aristotle University of Thessaloniki, Thessaloniki, Greece
[3] Meteorology and Air Quality Group, Wageningen University, Wageningen, The Netherlands
[4] Human Environment and Transport Inspectorate (ILT), Utrecht, The Netherlands
[5] Nanjing University of Information Science & Technology (NUIST), Nanjing, People's Republic of China

E-mail: ageor@auth.gr

OPEN ACCESS

RECEIVED
19 July 2020

REVISED
2 October 2020

ACCEPTED FOR PUBLICATION
23 October 2020

PUBLISHED
4 December 2020

Keywords: ships, pollution, NO_2, AIS, TROPOMI, wind

Supplementary material for this article is available online

Abstract

This paper presents an analysis of tropospheric NO_2 column measurements from the TROPOspheric Monitoring Instrument onboard the Copernicus Sentinel 5 Precursor satellite (TROPOMI/S5P) for an oceanic area in the central Mediterranean on 2 July 2018. The day and area were selected because of the stable and cloud-free weather conditions with low wind speeds throughout most of the area, while covering one of the busiest worldwide international shipping corridors. In addition, the area was affected by sunglint, i.e. sunlight that is directly reflected by the ocean surface waves to the satellite which greatly enhances the signal-to-noise ratio of the satellite observations. The satellite measurements reveal plume-like emission structures in tropospheric NO_2 columns while automated identification signal (AIS) data of ship locations reveal a total of 185 ships in the area. Combined with information about wind speed and wind direction within 3 h prior to the TROPOMI/S5P overpass, the ship tracks can almost perfectly be aligned with the plume-like tropospheric NO_2 structures. In addition, information about ship length and ship speed, combined with an analysis of ship tracks and ship position, reveal that nearly all emission plume-like tropospheric NO_2 structures can be attributed to the largest ships, mostly container ships and crude oil tankers. Overall, our results show for the first time ever that NO_2 emission plumes from ships can be detected and attributed to individual ships using satellite measurements, while also providing strong support for using satellite sunglint measurements.

1. Introduction

Ships at sea are strong emitters of nitrogen oxide (NO_x = NO + NO_2) and sulphur oxide (mostly SO_2) air pollution. Recent estimates by Johansson *et al* (2017) indicate that the global shipping fleet emitted a total of 6.4 Tg N to the atmosphere in the year 2015, which amounts to 13% of the global nitrogen (N) emissions (e.g. Miyazaki *et al* 2017). The emissions of ships lead to enhanced concentrations of regulated pollutants such as NO_2, SO_2, and particulate matter (Viana *et al* 2014, Jonson *et al* 2020). This air quality degradation is damaging to human health (e.g. Liu *et al* 2016) and contributes to excessive nitrogen deposition over ecosystems (e.g. Jägerbrand *et al* 2019).

To reduce the negative impact of ship emissions, the International Maritime Organization (IMO) has implemented progressive regulations to decrease the emissions from ships in the open ocean, as well as even stricter measures in four special emission control areas close to densely populated coastal regions. The IMO regulations within the so-called NECA and SECA (nitrogen and sulphur emission control areas) require that ships constructed after 1999 use engines that are compliant with NO_x emission limits (IMO MARPOL ANNEX VI—regulation 13 2020), and that all ships burn fuel with a sulphur content smaller than

0.5% (by mass) and smaller than 0.1% since 1 January 2020 (IMO MARPOL ANNEX VI—regulation 14 2020). This effectively prohibits the burning of low-grade quality ship fuels that were traditionally used in international shipping (Lack and Corbett 2012). However, fuel that is high in sulphur content is considerably cheaper than low sulphur fuels (Cullinane and Bergqvist 2014), inciting ship owners to circumvent the IMO regulations. How to globally monitor emissions and enforce regulation, especially over the vast open oceans, remains an outstanding question (SCIPPER 2020).

Current compliance monitoring includes port state authorities conducting checks of engine room logs and bunker delivery notes as well as taking fuel samples for a limited number of ships. On-board measurements at the ships exhaust pipes (Agrawal *et al* 2008), land- or ship-based downwind measurements of emission plumes using sniffer techniques (Lack *et al* 2009, Pirjola *et al* 2014) and the DOAS (differential optical absorption spectroscopy) approach (e.g. Mclaren *et al* 2012, Schreier *et al* 2015) are some of the methods currently used. Other methods comprise ship plume measurements from airborne platforms such as helicopters, small aircrafts, and drones (Van Roy and Scheldeman 2016). Mobile platforms typically measure pollutant (e.g. NO_x and SO_2) to CO_2 ratios during plume transects (Beecken *et al* 2014) or measure reflected skylight for remote optical sensing with the DOAS technique (Berg *et al* 2012). These methods require proximity to the ships monitored, are deployed infrequently, and are thus impractical or prohibitively expensive for checking the large number of ships sailing the world's oceans.

Earth observation satellites have the potential to play a key role here. So far, the spatial resolution and data quality of satellite sensors allowed for monitoring tropospheric NO_2 enhancements over the busiest shipping routes only after averaging months or years of data (e.g. Beirle *et al* 2004, Richter *et al* 2004, Vinken *et al* 2014, Georgoulias *et al* 2019). The temporal evolution of these enhancements has been observed and linked to temporal patterns of economic activity (de Ruyter de Wildt *et al* 2012, Boersma *et al* 2015). However, the capacity of satellite measurements to attribute observations to individual ships has not been demonstrated yet.

Since October 2017, the TROPOspheric Monitoring Instrument onboard the Copernicus Sentinel 5 Precursor satellite (TROPOMI/S5P) (Veefkind *et al* 2012) observes global pollution at a much higher spatial resolution (originally 7 km × 3.5 km at nadir and 5.5 km × 3.5 km since August 2019) than its spaceborne precursors (resolution ranging from 40 km × 320 km for the Global Ozone Monitoring Experiment onboard ERS-2 to 13 km × 24 km for the Ozone Monitoring Instrument onboard EOS AURA). The unique resolution and superior data quality have proven TROPOMI/S5P capable of pinpointing small local NO_2 sources such as individual power plants (Beirle *et al* 2019), gas compressor stations (van der A *et al* 2020) and daily city-scale emissions (Lorente *et al* 2019).

Here we show for the first time that satellite-based tropospheric NO_2 measurements from TROPOMI/S5P provide sufficient detail on NO_2 pollution to be traced back to the emissions from individual ships. By combining ship location data in the hours before and up to the satellite's overpass with wind direction and wind speed in the marine boundary layer along with an emission proxy based on ship length and speed we show that we can identify the individual ships or groups of ships that cause the observed NO_2 plumes.

2. Method

2.1. Satellite observations

TROPOMI/S5P (Veefkind *et al* 2012) was launched on 13 October 2017 and the operational phase started in April 2018. The instrument measures the top-of-the-atmosphere solar radiation reflected by and radiated from the Earth between 270–500 nm and 675–775 nm, and in the shortwave infrared. The two dimensions of the detector allow to simultaneously measure 450 spectra over the entire 2600 km strip, corresponding to a spatial resolution for individual pixels of 7 km (along) × 3.5 km (across) at nadir (5.5 km × 3.5 km since 6 August 2019). The equator crossing time is near 13:30 local solar time. For the scopes of this research, we use level-2 tropospheric NO_2 column data (version 1.2.2 and 1.3 data publicly available via https://s5phub.copernicus.eu/).

The NO_2 columns are retrieved with a three-step procedure described in the Algorithm Theoretical Baseline Document (van Geffen *et al* 2019). In the first step, NO_2 slant column densities, defined as the integrated amount of NO_2 along the average photon path from the Sun through the atmosphere back to the sensor, are obtained from the radiance and irradiance spectra using the DOAS technique in the 405–465 nm window (Boersma *et al* 2018, van Geffen *et al* 2020) where NO_2 has prominent spectral features. Then, the slant column is separated into a stratospheric and tropospheric part based on information from a data assimilation system (Dirksen *et al* 2011). Finally, the tropospheric slant columns are converted into tropospheric vertical column densities by application of a tropospheric air mass factor (AMF) based on a look-up table of altitude-dependent AMFs and actual information on surface and cloud characteristics, and on the vertical distribution of NO_2 predicted by the TM5-MP model on a 1° × 1° grid (Lorente *et al* 2017). TROPOMI/S5P tropospheric NO_2 columns show excellent correlation with independent aircraft and ground-based instruments but are biased low by about 30% (e.g. Lorente *et al* 2019, Verhoelst *et al* 2020).

2.2. Ship data

In 2000, IMO adopted the requirement for all ships to carry automatic identification systems (AIS) (IMO 1998, 2004, 2015). The regulations, in summary, prescribe that all vessels involved in commercial operations at sea are required to broadcast an AIS signal, including the ship's identity, type, position, course and speed among others. These data are frequently updated and broadcasted, typically every few seconds.

The broadcasted VHF signal can be received by land-based stations and satellites. Due to limited range of ground-based stations and the focus of this study on ship operations in the open sea, the most important data source is AIS signals received by satellites. In areas with high vessel density, an interference of messages may occur, constraining the reception of all broadcasted signals by a single satellite (Hoye 2004). However, part of this issue is resolved by over 60 satellites receiving AIS signals globally and the continuous technological improvement of receivers (Eriksen *et al* 2010).

Despite the relevance of these data for a wide range of public applications in the field of security, safety and the marine environment (Fournier *et al* 2018) there is no open access to satellite AIS data at the moment. AIS data are available from several commercial providers. Within the scope of this research, the Human Environment and Transport Inspectorate (ILT) was granted access to such sources.

While data in the AIS signal for identification, location, speed and heading are generally of good quality, additional information on for example ship dimensions are known to suffer from data and entry errors. To reduce errors in this study ship details regarding type and dimensions are retrieved from official ship registries.

2.3. Wind speed and direction

We use 10 m wind data from the European Center for Medium range Weather Forecasts (ECMWF). More specifically, wind fields (direction and speed) were taken from the ECMWF operational model analyses at a 0.25° resolution at 6-hourly timesteps. Assessment of this ECMWF wind speed product using observational data from spaceborne scatterometers has indicated a global low bias of $-0.4\ \mathrm{m\ s^{-1}}$ (Chelton and Freilich 2005), while locally, the ECMWF wind products can be biased up to $\pm\ 2\ \mathrm{m\ s^{-1}}$ (Belmonte and Stoffelen 2019, Trindade *et al* 2020).

2.4. Matching ships to observed NO_2 plumes

Here we use AIS ship location data in conjunction with quality assured tropospheric NO_2 data (qa_value > 0.5, cloud fraction < 0.5) from TROPOMI/S5P to attribute observed NO_2 enhancements on 2 July 2018 over a region in the central Mediterranean (dashed box area in figure 1(b)) to specific ships. This scene is selected from a large number of TROPOMI/S5P tropospheric NO_2 and ECMWF near surface wind field images for the 1-year period July 2018–June 2019. The observed features which are located in an area of busy shipping routes (figure 1(a)) and point directly to ship plumes along with an absence of clouds (clear-sky scenes identified via the retrieved effective cloud pressure; see section 1 of the electronic supplement for details and van der A *et al* 2020), calm wind conditions (limited dispersion of the ship plumes) and the fact that the TROPOMI/S5P measurements in the area were taken under sunglint viewing conditions (area defined as 'sunglint possible' by the TROPOMI algorithm; geolocation_flags = 2) make this day a perfect candidate for the scopes of this study (see figure 1(b)).

Sunglint is observed in satellite data when the satellite viewing zenith angle and solar zenith angle is such that the sunlight is directly reflected towards the sensor, and the sea surface is sufficiently calm, so the ocean 'acts' like a mirror. Indeed, the TROPOMI/S5P scene albedo values in figure 1(e) and the RGB image (figure 1(f)) at nearly the same time taken from the Visible Infrared Imaging Radiometer Suite onboard the Suomi National Polar-Orbiting Partnership (VIIRS/Suomi NPP) show that TROPOMI/S5P clearly observed sunglint. Satellite measurements taken in sunglint geometries have a significantly increased sensitivity to NO_2 close to the apparently bright surface as compared to non-glint geometries taken over a low albedo sea surface. This is illustrated in figure 1(c) showing higher normalized tropospheric slant columns (NO_2 slant column density/geometric AMF) and more distinct plumes in the sunglint scene southwest of Greece. TROPOMI's good sensitivity to NO_2 is further corroborated by the high scene albedo (figure 1(e) and section 1 of the electronic supplement) and associated tropospheric AMFs within the sunglint region (figure 1(d)). The dark spot appearing in the middle of the sunglint scene (figures 1(d)–(f)) is due to the very low wind conditions (see section 1 of the electronic supplement for details).

The spatial correspondence between NO_2 satellite-based measurements and ship locations is not trivial. The plume emitted by each ship will be advected by the prevailing winds and hence the NO_2 plume observed by TROPOMI/S5P will not necessarily coincide with the ship's track over the past hours. To attribute a plume to a particular ship, a simple 'morphing' technique is applied on the ship position data in order to calculate the position of the pollution plume at the time of S5P overpass (see figure S2 (available online at https://stacks.iop.org/ERL/15/124037/mmedia)). Assuming a NO_x lifetime of a few hours we use AIS ship coordinate data for the past 3 h prior to the S5P overpass (around 11:43 UTC) and wind speed and direction data at 10 m above sea level (asl) from the ECMWF for 12:00 UTC. The ship coordinates are collocated with the corresponding wind data. We assume that

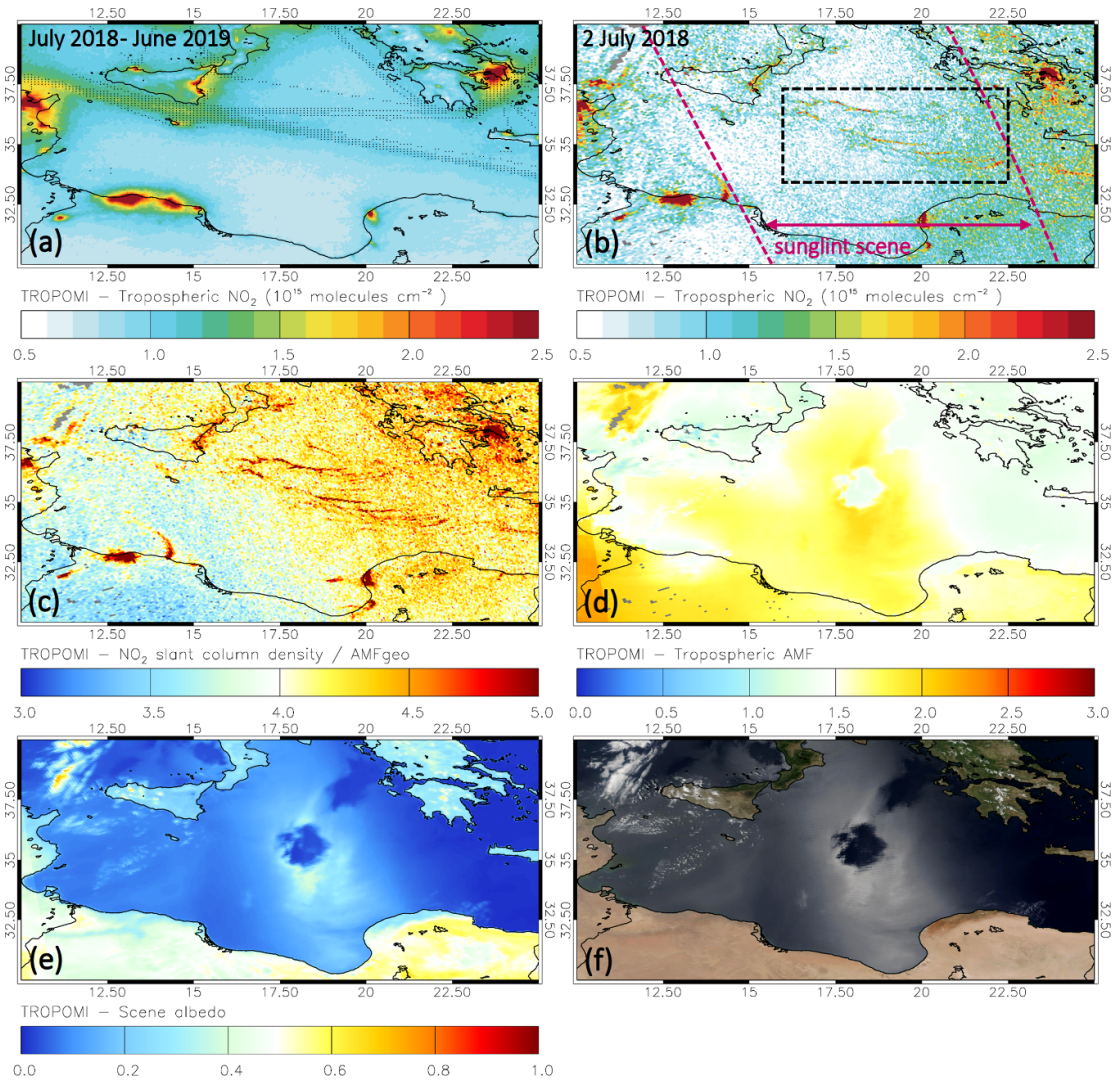

Figure 1. (a) Mean TROPOMI/S5P tropospheric NO_2 column (in 10^{15} molecules cm^{-2}) over the greater area of the central Mediterranean for the 1-year period July 2018–June 2019. The little dots indicate areas where the total CAMS NO_x ship emissions (Jalkanen *et al* 2016, Granier *et al* 2019) for 2018 are larger than 50 tonnes (busiest shipping routes). (b) TROPOMI/S5P tropospheric NO_2 column over the same area on 2 July 2018 when we observe ship plumes. The dashed box denotes the area of interest that encloses the observed ship plumes. The purple dashed lines indicate the portion of the swath wherein the viewing geometry has a high probability of sunglint ('sunglint possible'; geolocation_flags = 2 in the TROPOMI data product[6]). (c) TROPOMI/S5P normalized tropospheric slant column (NO_2 slant column density/geometric AMF) patterns, (d) Tropospheric AMF patterns and (e) Scene albedo for 2 July 2018. (f) VIIRS/Suomi NPP RGB image (https://worldview.earthdata.nasa.gov/) taken at nearly the same time with the TROPOMI/S5P retrievals.

the plume emitted at each ship position has travelled a distance $s = u \cdot |\Delta t|$ in the direction of the wind (the earth's curvature is taken into account) with a speed u equal to the wind speed at the ship location for a time period Δt (difference between the AIS time at the ship position and the S5P overpass time).

It has to be noted that the wind speed and direction is assumed fixed for each ship position during Δt; however, this is not very important here as wind speeds are generally low (mostly below 5 m s^{-1}) and wind speed and direction will not change significantly within the distances traveled by the ship plume on 2 July 2018. Plume dispersion and chemistry have not been accounted for and wind is assumed not to change with time and height. Despite these simplifications, our simple ship emission plume projections align well with the tropospheric NO_2 patterns observed by TROPOMI/S5P (see Results section and figure 2).

Finally, we match up the projected ship plumes with the TROPOMI/S5P tropospheric NO_2 column fields. This allows us to quantify the overall NO_2 pollution burden associated with each individual ship.

3. Results

Figure 2(a) shows the AIS ship coordinates located within the area of interest defined in figure 1(b) during the last 3 h before and up to TROPOMI's

[6]Lacking information on the smoothness of the water surface, a static criterion based on scattering angles (function of the zenith and azimuth angles of the sun and the spacecraft) being smaller than 18° is applied in the TROPOMI data product.

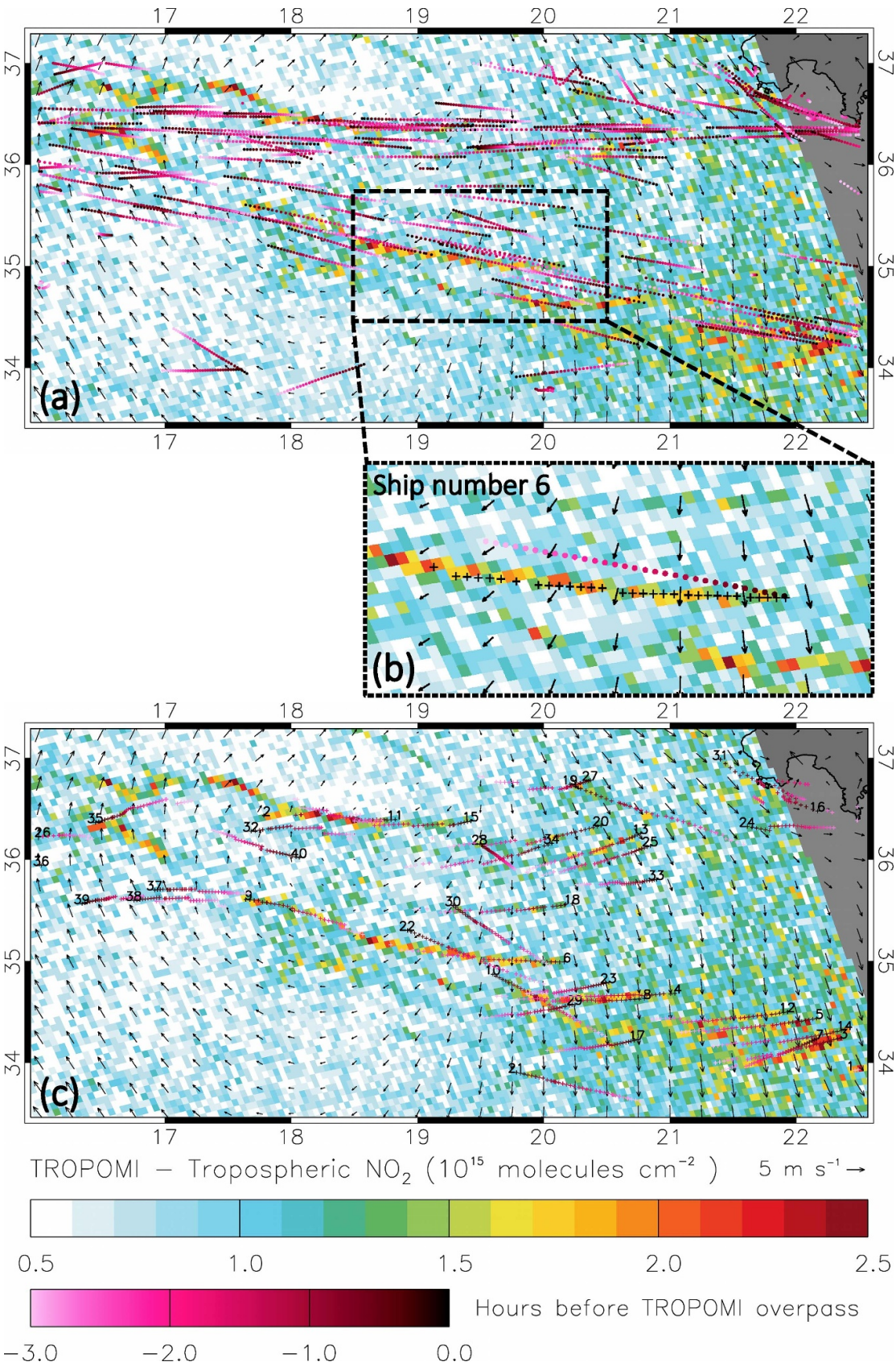

Figure 2. (a) TROPOMI/S5P tropospheric NO_2 patterns under sunglint viewing conditions, 10-meter wind fields from the ECMWF operational model analyses, and AIS ship locations the last 3 h before and up to TROPOMI's overpass time. Dark magenta colors are used for the ship positions close to the satellite's overpass time and brighter magenta colors for earlier ship positions. (b) An example of the original AIS locations (dots) and the projected plume locations (crosses) of a ship (Ship 6) at the time of TROPOMI's overpass. (c) The same as (a) but for the projected plumes of the 40 ships with L_s >200 m. The ships are numbered according to their NO_2 levels. Dark magenta colors are used for ship plumes emitted close to the satellite's overpass time and brighter magenta colors for earlier ship plumes.

overpass time. A total of 185 ships were found to sail in the greater area. The sailing direction of the ships can be identified, as dark magenta colors are used for the ship positions close to TROPOMI's overpass time and brighter magenta colors for earlier ship positions. Most of the ships follow two shipping routes (from and towards the Suez channel and the Black Sea), that do not exactly coincide with the observed TROPOMI/S5P NO_2 enhancements. This is to be expected as the plume originating from each ship is advected by the prevailing winds. The projected plumes, based on the AIS ship positions in the last 3 h and the ECMWF wind data, coincide much better with the observed NO_2 enhancements than the original AIS positions (figures 2(a) and S3). A striking example is shown in figure 2(b) where the original AIS locations and the corresponding projected plume for one specific ship are shown. This is a large (ship length; $L_s = \sim 334$ m) fast traveling (ship speed; $u_s = 19.7$ knots or else 36.5 km h^{-1}) container ship .

Despite the generally good colocation of the calculated plume locations of all the ships and the TROPOMI/S5P NO_2 enhancements, there are still a large number of ships that do not coincide with high NO_2 values; these are mostly small vessels (e.g. fishing boats). In order to identify which ships are indeed responsible for the observed NO_2 plumes we filtered the ships according to their length. Only ships with L_s >200 m were taken into account as smaller ships are expected to emit significantly less (see equation (1)). A total of 40 ships were identified in our study domain, mostly container ships and crude oil tankers (see figure 2(c)). Details about those 40 ships are provided in table S1 of the electronic supplement (length, vessel type, year built, gross tonnage, deadweight, and width usually referred as breadth).

Each calculated ship plume location was matched to the corresponding tropospheric NO_2 values seen in figure 2. The spatial average of the tropospheric NO_2 values coinciding with the plume of each ship was calculated and subsequently the ships were ranked according to their NO_2 levels. The individual ship number along with the average sailing speed and the corresponding NO_2 value are given in table S1. The effect of the ECMWF wind field uncertainty on the matching of ship plume locations and NO_2 is not significant as shown in section 2 of the electronic supplement.

Figure 2(c) shows that many of the observed NO_2 enhancements can be attributed to the pollution emitted by these large ships in the hours before the TROPOMI/S5P overpass. The use of ECMWF wind field data at 1000 hPa (~125 m asl) in the morphing returned similar results to the 10 m wind data, while the 950 hPa (~545 m asl) data performed much worse, (see figure 2(c) and figures S4 and S5) showing that at least for the very specific scene studied here the 10 m data are representative of the wind fields within the lower boundary layer. The AIS locations and the calculated plumes of each individual ship separately are given in figures S6-S45. Figure 2(c) also shows that TROPOMI detects relatively high NO_2 concentrations over areas where the plumes of more than one ship coincide (e.g. Ships 2, 11 and 15) or cross (e.g. Ships 22 and 6) and in mixed cases of clusters of ships, mostly over areas with higher wind speeds (around 5 m s^{-1}) (e.g. Ships 3, 7 and 14). In these cases, it is difficult to disentangle the relative contribution of the individual ships to the observed NO_2 levels. However, apart from those cases there are ships (e.g. Ships 9 and 18) which are totally isolated, and their projected plumes coincide well with the observed NO_2 plumes. These ships mostly sail in calm waters (wind speeds smaller than ~3 m s^{-1}) where dispersion by the wind is limited and the NO_2 plumes appear as long and narrow enhancements relative to the background. Taking this into account, the 40 largest ships were separated into three classes: (1) isolated ship plumes, (2) plumes in close proximity to other ships' plumes (clusters) and (3) plumes crossing other ships' plumes (see also table S1) based on a visual assessment including wind speed and direction.

To gain more insight into the sensitivity of TROPOMI/S5P for detecting ship emissions we use a NO_x emission proxy E_s (see appendix A for details) which is given by:

$$E_s = L_s^2 \times u_s^3 \quad (1)$$

The advantage of E_s over other ship emission proxies (e.g. Fan *et al* 2016) is that it can be derived solely based on AIS data, while other reported emission proxies require additional information not contained in the AIS data. As u_s may change with time, E_s is calculated for each AIS ship location and then an average value is calculated per ship taking into account only locations which were previously matched to a TROPOMI/S5P pixel. The average E_s values for the 40 major ships in the area are given in table S1. Obviously, there are other factors affecting emissions which are not incorporated in equation (1), such as engine age, propulsion efficiency, fuel type and the loading level (ships emit more when fully loaded and maintaining the same speed). Here, E_s is used as a proxy for ship emission intensity bearing in mind the aforementioned uncertainties.

In figure S46 we show the tropospheric NO_2 levels (thick black line and dots) averaged over the calculated plume of each major ship in the area along with the ships' emission proxy E_s values (bars). We see that high NO_2 levels tend to coincide with higher E_s values (Pearson correlation coefficient R of 0.62); however, this is not very clear due to mixing individual ships with clusters of ships or ships crossing other ship's plume. For example, a ship with lower emission intensity sailing in parallel or close to one or more ships with high emissions will exhibit high NO_2

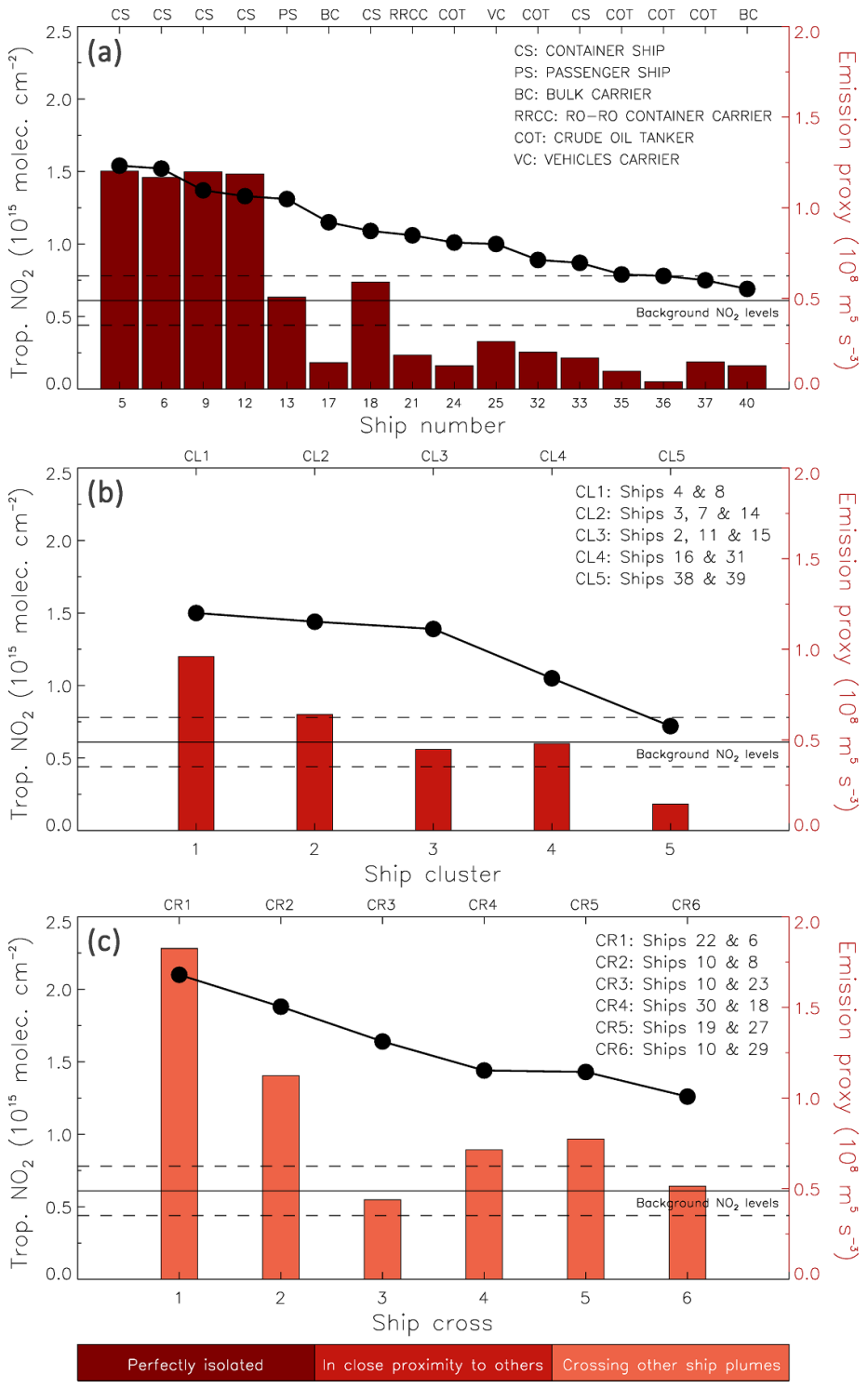

Figure 3. (a) TROPOMI/S5P tropospheric NO_2 levels (thick black line and dots) coinciding with the projected plumes of the largest isolated ships in the area (L_s > 200 m) and the corresponding average emission proxy (E_s) values (bars). The ships are ranked according to their NO_2 levels. The type of each ship is also given. The background tropospheric NO_2 in the area (average for the clean ship-free box area confined between 16–17° E and 34–35° N) is indicated with a thin black line while the dashed lines denote the $\pm 1\sigma$. (b) The same as (a) but for the average NO_2 levels over clusters of ships in the area with the corresponding average E_s values. The ships that form each cluster are defined. (c) The same as (a) but for NO_2 measurements corresponding to the central pixel where ship plumes cross and the corresponding cumulative E_s values. The pairs of crossing ships are defined.

values but low E_s values. To avoid such a confusion, the NO_2-E_s relations are studied for each ship class separately.

Figure 3(a) shows the NO_2 levels that coincide with the projected plumes of the perfectly isolated ships (thick black line and dots) and the average E_s values (bars). It should be noted that Ships 1 and 26 were filtered out as only a part of their projected plume is within the study domain (corresponding only to AIS locations 2 to 3 h prior to the

TROPOMI/S5P overpass). We see that there is a good correlation between the observed tropospheric NO_2 and E_s ($R = 0.88$).

In figure 3(b) the average NO_2 levels over clusters of ships in the area with the corresponding average E_s values are presented. More specifically, five clusters were identified (Cluster 1: Ships 4 and 8, Cluster 2: Ships 3, 7 and 14, Cluster 3: Ships 2, 11 and 15, Cluster 4: Ships 16 and 31 and Cluster 5: Ships 38 and 39). A good correlation between the tropospheric NO_2 and the E_s values is seen, similarly to the isolated ships.

Figure 3(c) shows the tropospheric NO_2 levels at locations where pairs of ship plumes are crossing. A total of ten crossings were first identified in figure 2(c). The crossing coordinates for each ship are calculated by minimizing the distance between the projected plumes of a pair of ships. However, due to the spatiotemporal resolution of the AIS data used here, only in six cases the crossing coordinates of ships were falling within the same TROPOMI/S5P pixel. Hence, six crossing cases are finally reported (Crossing 1: Ships 22 and 6, Crossing 2: Ships 10 and 8, Crossing 3: Ships 10 and 23, Crossing 4: Ships 30 and 18, Crossing 5: Ships 19 and 27 and Crossing 6: Ships 10 and 29). For each pair of ships, the NO_2 values appearing in figure 3(c) are the measurements corresponding to the central pixel where the two ship plumes cross. Assuming that the NO_2 in this pixel is a consequence of the emissions of both ships, the corresponding E_s values in figure 3(c) are the sum of the E_s values of the two ships at the crossing coordinates (cumulative E_s). Again, we see that tropospheric NO_2 values follow the variability of E_s well.

The overall good correlation between TROPOMI/S5P NO_2 and E_s for all the three cases together ($R = 0.85$) suggests that the enhanced NO_2 columns observed here are indeed due to emissions from the largest and fast-sailing ships in the area. It should be noted that the younger ships examined here (constructed after 1 January 2011; Tier II emission standards) are on average larger and sail faster exhibiting higher NO_2 levels (see table S1 and discussion in section 3 of the electronic supplement).

Finally, we also applied a longitude-dependent background correction to the NO_2 data to distinguish the tropospheric NO_2 column enhancement due to shipping emissions from the free tropospheric background or residual boundary-layer NO_2 (see section 3 of the electronic supplement for details). Our results did not change significantly (ships, clusters of ships or crossing ships with higher E_s values generally coincide with higher NO_2 levels as shown in figure S47 with an overall R value of 0.85). This suggests that for the scene we study here a background correction is not vital; however, we acknowledge that for other scenes or areas with higher background NO_2 a correction could be necessary.

4. Discussion

The results presented here show that: (1) ship emission plume-like structures can be observed in daily TROPOMI/S5P NO_2 columns over the central Mediterranean under sunglint conditions, (2) these structures remain after division of the NO_2 slant column densities by the geometrical AMFs, and thus are not an artifact of the retrieval algorithm, (3) these structures can be aligned with ship plumes when morphing the 3 h ship tracks before the TROPOMI/S5P overpass time with the prevailing near surface winds, and (4) these plume structures appear to be best detectable for the largest ships. In addition, results are robust with regard to uncertainties in wind speeds used for projecting the ship plumes.

Our results indicate that ships frequently travel along the same shipping lane but occasionally ship tracks also cross each other. As a result, emissions mix and attribution of tropospheric NO_2 column values to emissions of a single ship becomes complicated. In our analysis we identified isolated ship plumes by visual inspection, but the need for a more objective method in future studies is acknowledged.

Our results also show that TROPOMI/S5P can track emission plumes from the largest ships, or aggregates of smaller ships whose emissions merge, resulting in detectable NO_2 enhancements. More research using more TROPOMI/S5P scenes and thus exploring more ship types should provide better statistics on the detection limits of ships from TROPOMI/S5P data. This information is also relevant for future satellite missions like the Copernicus Anthropogenic Carbon Dioxide Monitoring CO_2M (Sierk *et al* 2019) that plan to measure tropospheric NO_2 columns at higher spatial resolutions.

In addition, an outstanding question remains under what atmospheric conditions ship plumes can be best detected. The effect of viewing geometries and wind speed, which affects both surface reflectance under sunglint as well as plume dispersion and humidity, should be investigated in more detail. Also, the detectability of NO_2 pollution plumes from individual ships over different areas around the globe (e.g. open seas, ports and shorelines) should be studied.

Undoubtedly, the detection of ship plumes under favorable conditions only is a limitation of satellite remote sensing. A 1-year (July 2018–June 2019) analysis we did for the Mediterranean Sea (see section 4 of the electronic supplement for details) showed that the possibility of having conditions like the ones in the scene studied here (i.e. quality assured cloud-free NO_2 retrieval under sunglint viewing geometry and near surface wind speeds less than 5 m s^{-1}) is ∼5%–10% on an annual basis (figure. S48(b)). The majority of sunglint viewing scenes over the area appear in summer, less appear in spring and much lesser in autumn. For sunglint conditions only (regardless of the wind speed) the possibility increases

to ∼10%–15% (figure S48(a)). For low wind speed conditions only (under all viewing geometries) the possibility is much higher, exceeding 50% in some coastal areas (figure S48(d)).

In our study we rely on a simple ship emission proxy based on ship length and speed. However, there are many factors that determine ship emission such as hull shape, engine type, fuel type, and weight which is not captured by the emission proxy formula. Modelling ship engine performance and emissions is an active field of engineering research (e.g. Jalkanen *et al* 2012, Johansson *et al* 2017) and such models could be used to better estimate ship emissions based on ship characteristics.

In turn, the possibility of TROPOMI/S5P and future satellite missions to start monitoring emissions from individual ships should be of great value for verification of ship engine performance and emission modelling. This is very important as the shipping sector is expected to grow making emission control and monitoring more challenging (Rogelj *et al* 2018). In addition, the use of updated ship emissions in climate modeling studies would allow for more accurate projections of climate's current state and future.

Finally, although not shown and discussed here, we have consistently observed similar patterns in daily TROPOMI/S5P data under sunglint conditions throughout the Mediterranean. Performing a global assessment will drastically increase the number of events available for analysis. Many more cases will allow for a much more detailed systematic analysis of various findings of our paper and issues discussed here.

5. Concluding remarks

We have shown for the first time that NO_2 pollution plumes can be observed in single overpass TROPOMI/S5P tropospheric NO_2 column data under favorable conditions (cloud-free skies, low winds and sunglint) and can be attributed to emissions from large individual ships as well as groups of ships sailing in close proximity. Our findings open up a new avenue for analysis and development of applications, including ship emission monitoring for regulation compliancy. This is particularly important, as there are global efforts underway to define regulations to reduce air pollution emissions from shipping.

Appendix A

Ship emissions to first order depend on the ship's speed (resistance) and its water displacement or volume. In fluid dynamics, resistance depends on the square of the speed (u_s^2). The water resistance of a ship traveling through water is proportional to $A_s \times u_s^2$ where A_s is the area of the ship and u_s its speed. The impulse of a moving ship through water then equals u_s multiplied by the resistance, so the impulse is proportional to $A_s \times u_s^3$ (Fan *et al* 2016).

For large international ships the length-width-height dimensions and ratios are not expected to vary that much, if only because ship design focuses on efficiency as fuel is a dominant cost in international shipping. Logically, ship designs are expected to be rather similar. Hence, the ship area A_s is then to first order expected to be proportional to the square of the ship length ($A_s \sim L_s^2$), which also has an area dimension. Combined, we come up with an emission proxy E_s of $L_s^2 \times u_s^3$. A speed-to-the-power-three relation is also consistent with findings from a computation study on ship engine performance and emission parameters mapping (Theokatos and Tzelepis 2015).

Acknowledgments

This research was funded by the First Assessment of Shipping emissions in TROPOMI data (FAST) project financed by the AOMD (Anders Omgaan Met Data) program (2015-2019) of the Dutch Ministry of Infrastructure and Water Management and the AVES-Oculus project of the Dutch Ministry of Infrastructure and Water Management. Part of AKG's work was funded by the project 'PANhellenic infrastructure for Atmospheric Composition and climatE change' (MIS 5021516) which is implemented under the Action 'Reinforcement of the Research and Innovation Infrastructure', funded by the Operational Programme 'Competitiveness, Entrepreneurship and Innovation' (NSRF 2014-2020) and co-financed by Greece and the European Union (European Regional Development Fund). Part of this work (JvV) was supported by the SCIPPER project which has received funding from the European Union's Horizon 2020 research and innovation programme under grant agreement Nr.814893. The authors thank Jos van Geffen (KNMI) and Christoph Riess (WUR) for providing valuable information for the paper.

Data availability statement

The tropospheric NO_2 data (version 1.2.2 and 1.3) used here are publicly available via the Copernicus S5P hub (https://s5phub.copernicus.eu/). The AIS data were provided by the Human Environment and Transport Inspectorate (ILT). The wind field data were extracted from ECMWF (https://www.ecmwf.int/). The emission data used in figure 1(a) are publicly available through the ECCAD web repository (https://eccad3.sedoo.fr). The VIIRS image in figure 1(e) was acquired through NASA worldview (https://worldview.earthdata.nasa.gov/).

Author contributions

AKG is the main author of the paper and performed the data analysis. KFB contributed to the

data analysis and interpretation and co-authored the paper. JvV provided the AIS data, contributed to the data analysis and interpretation and co-authored the paper. RvdA and XZ provided the ship emission proxy formula derived from an ongoing research project and commented on the paper. PZ provided research budget (PANACEA) and commented on the paper. JdL provided research budget (AOMD), contributed to the data analysis and interpretation and co-authored the paper.

References

Agrawal H, Malloy Q G J, Welch W A, Wayne Miller J and Cocker D R 2008 In-use gaseous and particulate matter emissions from a modern ocean going container vessel *Atmos. Environ.* **42** 5504–10

Beecken J, Mellqvist J, Salo K, Ekholm J and Jalkanen J-P 2014 Airborne emission measurements of SO_2, NO_x and particles from individual ships using a sniffer technique *Atmos. Meas. Tech.* **7** 1957–68

Beirle S, Borger C, Dörner S, Li A, Hu Z, Liu F, Wang Y and Wagner T 2019 Pinpointing nitrogen oxide emissions from space *Sci. Adv.* **5** eaax9800

Beirle S, Platt U, von Glasow R, Wenig M and Wagner T 2004 Estimate of nitrogen oxide emissions from shipping by satellite remote sensing *Geophys. Res. Lett.* **31** L18102

Belmonte Rivas M and Stoffelen A 2019 Characterizing ERA-Interim and ERA5 surface wind biases using ASCAT *Ocean Sci.* **15** 831–52

Berg N, Mellqvist J, Jalkanen J-P and Balzani J 2012 Ship emissions of SO_2 and NO_2 : DOAS measurements from airborne platforms *Atmos. Meas. Tech.* **5** 1085–98

Boersma K F *et al* 2018 Improving algorithms and uncertainty estimates for satellite NO_2 retrievals: results from the quality assurance for the essential climate variables (QA4ECV) project *Atmos. Meas. Tech.* **11** 6651–78

Boersma KFolkert, Vinken GC and Tournadre J 2015 Ships going slow in reducing their NOx emissions: changes in 2005–2012 ship exhaust inferred from satellite measurements over Europe *Environ. Res. Lett.* **10** 074007

Chelton D B and Freilich M H 2005 Scatterometer-based assessment of 10-m wind analyses from the operational ECMWF and NCEP numerical weather prediction models *Mon. Wea. Rev.* **133** 409–29

Cullinane K and Bergqvist R 2014 Emission control areas and their impact on maritime transport *Transp. Res.* D **28** 1–5

de Ruyter de Wildt M, Eskes H and Boersma K F 2012 The global economic cycle and satellite-derived NO $_2$ trends over shipping lanes *Geophys. Res. Lett.* **39** L01802

Dirksen R J, Boersma K F, Eskes H J, Ionov D V, Bucsela E J, Levelt P F and Kelder H M 2011 Evaluation of stratospheric NO_2 retrieved from the Ozone Monitoring Instrument: intercomparison, diurnal cycle, and trending *J. Geophys. Res.* **116** D08305

Eriksen T, Skauen A N, Narheim B, Helleren O, Olsen O and Olsen R B 2010 Tracking ship traffic with space-based AIS: experience gained in first months of operations *2010 Int. WaterSide Security Conf.* (WSS) (Carrara: IEEE) pp 1–8 (https://ieeexplore.ieee.org/document/5730241/)

Fan Q, Zhang Y, Ma W, Ma H, Feng J, Yu Q, Yang X, Ng S K W, Fu Q and Chen L 2016 Spatial and seasonal dynamics of ship emissions over the Yangtze river delta and East China sea and their potential environmental influence *Environ. Sci. Technol.* **50** 1322–9

Fournier M, Casey Hilliard R, Rezaee S and Pelot R 2018 Past, present, and future of the satellite-based automatic identification system: areas of applications (2004–2016) *WMU J. Marit. Affairs* **17** 311–45

Georgoulias A K, van der A R J, Stammes P, Boersma K F and Eskes H J 2019 Trends and trend reversal detection in 2 decades of tropospheric NO $_2$ satellite observations *Atmos. Chem. Phys.* **19** 6269–94

Granier C *et al* 2019 The Copernicus Atmosphere Monitoring Service global and regional emissions Report April 2019 version null Accessed September 2020

Hoye G 2004 Ship detection probability analysis for a possible long-range AIS system FFI/Report-2004/04383 (available at: http://rapporter.ffi.no/rapporter/2004/04383.pdf Accessed September 2020)

IMO MARPOL ANNEX VI - regulation 13 2020 (available at: www.imo.org/en/OurWork/Environment/PollutionPrevention/AirPollution/Pages/Nitrogen-oxides-(NOx)—Regulation-13.aspx Accessed September 2020)

IMO MARPOL ANNEX VI - regulation 14 2020 (available at: www.imo.org/en/OurWork/Environment/PollutionPrevention/AirPollution/Pages/Sulphur-oxides-(SOx)—Regulation-14.aspx Accessed September 2020)

IMO 1998 Resolution MSC.74(69) Recommendation on Performance Standards for Universal Automatic Identification System (AIS) (available at: www.imo.org/en/KnowledgeCentre/IndexofIMOResolutions/Maritime-Safety-Committee-(MSC)/Documents/MSC.74(69).pdf Accessed September 2020)

IMO 2004 (available at: www.imo.org/en/OurWork/Safety/Navigation/Pages/AIS.aspx Accessed September 2020)

IMO 2015 Resolution A.1106(29) Revised Guidelines for the onboard operational use of shipborne automatic identification systems (AIS) (available at: www.imo.org/en/KnowledgeCentre/IndexofIMOResolutions/Assembly/Documents/A.1106(29).pdf Accessed September 2020)

Jägerbrand A K, Brutemark A, Barthel Svedén J and Gren I-M 2019 A review on the environmental impacts of shipping on aquatic and nearshore ecosystems *Sci. Total Environ.* **695** 133637

Jalkanen J-P, Johansson L and Kukkonen J 2016 A comprehensive inventory of ship traffic exhaust emissions in the European sea areas in 2011 *Atmos. Chem. Phys.* **16** 71–84

Jalkanen J-P, Johansson L, Kukkonen J, Brink A, Kalli J and Stipa T 2012 Extension of an assessment model of ship traffic exhaust emissions for particulate matter and carbon monoxide *Atmos. Chem. Phys.* **12** 2641–59

Johansson L, Jalkanen J-P and Kukkonen J 2017 Global assessment of shipping emissions in 2015 on a high spatial and temporal resolution *Atmos. Environ.* **167** 403–15

Jonson J E, Gauss M, Schulz M, Jalkanen J-P and Fagerli H 2020 Effects of global ship emissions on European air pollution levels *Atmos. Chem. Phys.* **20** 11399–422

Lack D A *et al* 2009 Particulate emissions from commercial shipping: chemical, physical, and optical properties *J. Geophys. Res.* **114** D00F04

Lack D A and Corbett J J 2012 Black carbon from ships: a review of the effects of ship speed, fuel quality and exhaust gas scrubbing *Atmos. Chem. Phys.* **12** 3985–4000

Liu H, Fu M, Jin X, Shang Y, Shindell D, Faluvegi G, Shindell C and He K 2016 Health and climate impacts of ocean-going vessels in East Asia *Nat. Clim. Change* **6** 1037–41

Lorente A *et al* 2017 Structural uncertainty in air mass factor calculation for NO $_2$ and HCHO satellite retrievals *Atmos. Meas. Tech.* **10** 759–82

Lorente A, Boersma K F, Eskes H J, Veefkind J P, van Geffen J H G M, de Zeeuw M B, Denier van der Gon H A C, Beirle S and Krol M C 2019 Quantification of nitrogen oxides emissions from build-up of pollution over Paris with TROPOMI *Sci. Rep.* **9** 20033

Mclaren R, Wojtal P, Halla J D, Mihele C and Brook J R 2012 A survey of NO_2: SO_2emission ratios measured in marine vessel plumes in the Strait of Georgia *Atmos. Environ.* **46** 655–8

Miyazaki K, Eskes H, Sudo K, Boersma K F, Bowman K and Kanaya Y 2017 Decadal changes in global surface NO_x emissions from multi-constituent satellite data assimilation *Atmos. Chem. Phys.* **17** 807–37

Pirjola L, Pajunoja A, Walden J, Jalkanen J-P, Rönkkö T, Kousa A and Koskentalo T 2014 Mobile measurements of ship emissions in two harbour areas in Finland *Atmos. Meas. Tech.* **7** 149–61

Richter A, Eyring V, Burrows J P, Bovensmann H, Lauer A, Sierk B and Crutzen P J 2004 Satellite measurements of NO_2 from international shipping emissions *Geophys. Res. Lett.* **31** L23110

Rogelj J D *et al* 2018 Mitigation pathways compatible with 1.5 °C in the context of sustainable development *Global Warming of 1.5 °C. An IPCC Special Report on the Impacts of Global Warming of 1.5 °C above Pre-industrial Levels and Related Global Greenhouse Gas Emission Pathways, in the Context of Strengthening the Global Response to the Threat of Climate Change, Sustainable Development, and Efforts to Eradicate Poverty* ed V Masson-Delmotte *et al* accepted (https://www.ipcc.ch/site/assets/uploads/sites/2/2019/02/SR15_Chapter2_Low_Res.pdf)

Schreier S F, Peters E, Richter A, Lampel J, Wittrock F and Burrows J P 2015 Ship-based MAX-DOAS measurements of tropospheric NO_2 and SO_2 in the South China and Sulu Sea *Atmos. Environ.* **102** 331–43

SCIPPER 2020 (available at: www.scipper-project.eu/ Accessed September 2020)

Sierk B, Bezy J-L, Löscher A and Meijer Y 2019 The European CO_2 Monitoring Mission: observing anthropogenic greenhouse gas emissions from space *Proc. SPIE* **11180** 237–50

Theotokatos G and Tzelepis V 2015 A computational study on the performance and emission parameters mapping of a ship propulsion system *Proc. IMechE* **229** 58–76

Trindade A, Portabella M, Stoffelen A, Lin W and Verhoef A 2020 ERAstar: a high-resolution ocean forcing product *IEEE Trans. Geosci. Remote Sens.* **58** 1337–47

van der A R J, de Laat A T J, Ding J and Eskes H J 2020 Connecting the dots: nOx emissions along a West Siberian natural gas pipeline *Npj Clim. Atmos. Sci.* **3** 16

van Geffen J, Boersma K F, Eskes H, Sneep M, Ter Linden M, Zara M and Veefkind J P 2020 S5P TROPOMI NO_2 slant column retrieval: method, stability, uncertainties and comparisons with OMI *Atmos. Meas. Tech.* **13** 1315–35

van Geffen J, Eskes H, Boersma K F, Maasakkers J D and Veefkind J P 2019 TROPOMI ATBD tropospheric and total NO_2 (available at: http://wXww.tropomi.eu/sites/default/files/files/publicS5P-KNMI-L2-0005-RP-ATBD_NO2_data_products-20190206_v140.pdf Accessed September 2020)

Van Roy W and Scheldeman K 2016 Best practices airborne MARPOL Annex VI monitoring *CompMon* (available at: https://compmon.eu/ Accessed September 2020)

Veefkind J P *et al* 2012 TROPOMI on the ESA Sentinel-5 Precursor: A GMES mission for global observations of the atmospheric composition for climate, air quality and ozone layer applications *Remote Sens. Environ.* **120** 70–83

Verhoelst T *et al* 2020 Ground-based validation of the Copernicus Sentinel-5p TROPOMI NO_2 measurements with the NDACC ZSL-DOAS, MAX-DOAS and Pandonia global networks *Atmos. Chem. Phys. Discuss.* (in review)

Viana M, Hammingh P, Colette A, Querol X, Degraeuwe B, Vlieger I D and van Aardenne J 2014 Impact of maritime transport emissions on coastal air quality in Europe *Atmos. Environ.* **90** 96–105

Vinken G C M, Boersma K F, van Donkelaar A and Zhang L 2014 Constraints on ship NO × emissions in Europe using GEOS-Chem and OMI satellite NO $_2$ observations *Atmos. Chem. Phys.* **14** 1353–69